Impedance Control for Critically Coupled Cavities

Bill Riddle and Craig Nelson
National Institute of Standards and Technology
325 Broadway
Boulder, CO 80305-3328
Email: Bill.Riddle@nist.gov

***Abstract*— Cavity resonators are often used in low phase noise oscillators that utilize carrier suppression. These oscillators are employed in systems that measure phase noise in frequencies as high as 100 GHz. In order to achieve the maximum suppression needed in these low noise designs, the cavity must be operated at critical coupling. However, this large coupling level loads the cavity, which significantly lowers its quality factor and shifts its resonant frequency. In this paper, we present a matching technique that can be used to minimize these loading effects by controlling the input impedance of the cavity and optimizing its response at resonance, thus producing the maximum amount of carrier suppression.**

I. Introduction

Research conducted recently at the National Institute of Standards and Technology (NIST) successfully employed an air-dielectric cavity as part of a discriminator circuit in a low phase noise oscillator design [1]. An integral part of this circuit's signal processing utilized the reflected signal of the resonant cavity to accomplish carrier suppression of the input signal to the cavity. Carrier suppression methods fulfill an important role in systems designed to measure or control the phase noise of signals [2]–[5]. When resonant cavities are used in these schemes, they are generally required to operate at critical coupling to achieve the desired performance. With respect to the cavity design utilized in [1], we present in this paper an alternative approach to achieving carrier suppression by compensating for the effects of critical coupling with a matching network at the input of the cavity. Based on a simplified circuit model of the cavity's resonant mode, we identify an input reference plane that allows us to compute the cavity's input impedance and reflection coefficient. From this, the cavity's response in both magnitude and phase can be optimized (i.e., the input reflected signal at resonance equals zero.) For demonstration purposes, data measured with two different cavities operating at different frequencies and resonant modes are presented with theoretically derived results for comparison.

Concerning notation, phasors are indicated with overhead carets and numbered equations are refered to with parentheses.

II. Description of the System Design

The basic design of the system analyzed in this paper is shown in simplified form in Fig. 1. The wave-guiding structure for this circuit is a 50 Ω coaxial transmission line, assumed to be lossless. The resonant device is a two-port, air-filled cylindrical cavity, constructed of aluminum and plated internally with silver and polished. A coaxial T-junction is connected to either the input or output port of the cavity, and a variable phase shifter is connected to the third port of the T-junction as shown in Fig. 1. Isolation and signal processing at the cavity's ports are provided by circulators and isolators. Coupling to the cavity is provided by loops constructed from the center conductors of the coaxial lines.

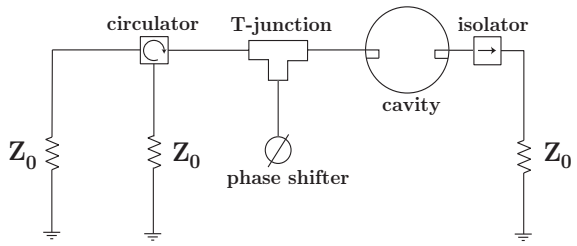

Fig. 1. Simplified diagram of the cavity circuit with input matching. Z_0 is the system's characteristic impedance.

III. Circuit Model of Resonant Cavity Mode

For time-harmonic signals excited within lossless coaxial lines, we know from transmission line theory [6] that electromagnetic fields propagate in the TEM mode and generate travelling wave voltages defined by

$$\widehat{V}(z) = \widehat{V}_m^+ e^{-\jmath\beta z} + \widehat{V}_m^- e^{\jmath\beta z},$$

where the z axis is aligned with the coaxial center conductor as the direction of propagation, and β is the propagation constant. The line impedance is given by

$$\widehat{Z}(z) = Z_0 \frac{1+\widehat{\Gamma}(z)}{1-\widehat{\Gamma}(z)},$$

with Z_0 as the characteristic impedance of the line (real for lossless lines) and $\widehat{\Gamma}$ as the reflection coefficient. Since these quantities depend on the axial variable z, we must designate a fixed reference plane in order to analyze the cavity's resonant mode. This allows the resonance to be described with an equivalent circuit model, which combines a frequency domain analysis with phasor quantities. In this paper, the reference plane (located at $z = z_L$ in Fig. 2) corresponds to the cavity's input connector.

Equivalent circuit models have been used successfully by many researchers to analyze the resonant modes of a microwave cavity and their coupled interactions with input and

0-7803-9052-0/05/$20.00 © 2005 IEEE.

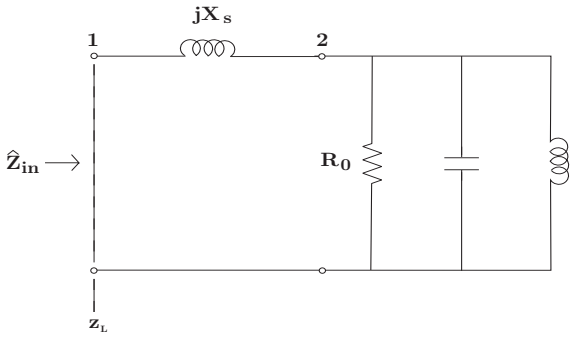

Fig. 2. Circuit diagram used to analyze the cavity mode with a parallel resonant circuit. X_s represents the coupling loop inductance. The input reference plane is located at $z = z_L$, which represents the input connector to the cavity.

output signals [7]–[10]. Recently, Kajfez [11] introduced an improved model of a one-port cavity that includes the effects of a coupling loop on the cavity's input impedance. In the design shown in Fig. 1, the output port coupling is very small (i.e., $\ll 1$) so we can, without loss of generality, use Kajfez's one-port model to explain the performance of the two-port cavity. Two-port models can be used to apply the techniques developed in this paper for more extensive results [12]–[14].

The one-port model used in our analysis is shown in Fig. 2. Two terminal nodes are used to distinguish the coaxial input to the cavity (labeled as 1) and a parallel resonant circuit representing the cavity mode (labeled as 2.) The coupling loop is modeled as a series inductive reactance X_s, assumed constant over the bandwidth of the cavity's frequency response (legitimate for high Q cavities.) The resonant circuit impedance is shown with real part R_0 and the cavity parameters Q_0 and f_0 (unloaded Q and resonant frequency) are represented by the parallel capacitor-inductor combination. From the circuit model, the unloaded input impedance is given by

$$\widehat{Z}_{in}(f)\Big|_{z=z_L} = \jmath X_s + R_0 \left(1 + \jmath 2Q_0 \frac{f - f_0}{f_0}\right)^{-1}. \quad (1)$$

Equation (1) is an approximation to the input impedance that could be measured by a network analyzer with a calibration plane at z_L. Also, this expression was derived under the assumption that the frequency bandwidth $\Delta f \ll f_0$, which is generally true for high Q cavities.

In practice, the cavity must be connected to an external circuit with characteristic impedance Z_0, as shown in Fig. 3. The combined loading effect of the loop reactance and the external circuit on the cavity mode can be analyzed by calculating the reflection coefficient at node 2 in Fig. 3. This reflection coefficient is given by

$$\widehat{\Gamma}_{in}(f) = \widehat{\Gamma}_d \left[1 - \frac{2\kappa}{1+\kappa} \cdot \frac{1}{1 + \jmath 2Q_L \left(\frac{f - f_L}{f_0}\right)}\right], \quad (2)$$

where the coupling coefficient κ is defined by

$$\kappa = \frac{R_0/Z_0}{1 + (X_s/Z_0)^2}. \quad (3)$$

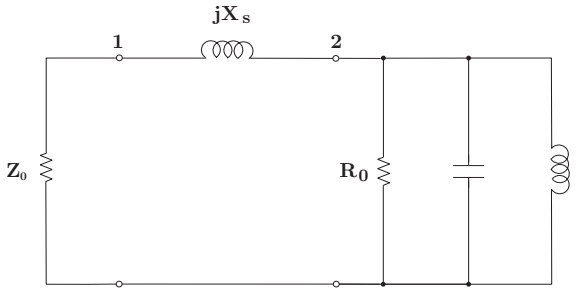

Fig. 3. Loaded circuit representing the resonant cavity when attached to an external system with characteristic impedance Z_0. The reflection coefficient $\widehat{\Gamma}_{in}$ is calculated at node 2.

The constant $\widehat{\Gamma}_d$, defined as the detuned reflection coefficient, is the asymptotic value of $\widehat{\Gamma}_{in}$ for frequencies far from the resonant frequency f_0, such that

$$\widehat{\Gamma}_d = \frac{\jmath X_s - Z_0}{\jmath X_s + Z_0}. \quad (4)$$

The loaded values for Q and resonant frequency are given by

$$Q_L = \frac{Q_0}{1+\kappa} \quad (5)$$

$$f_L = f_0 \left(1 + \frac{\kappa X_s}{2Q_0 Z_0}\right). \quad (6)$$

IV. Conditions for Optimum Response

In order to produce the maximum amount of carrier suppression needed for low phase noise oscillators, the cavity must be engineered to operate optimally at its unloaded resonant frequency. From the equations presented in the previous section using the circuit model in Fig. 3, this means that $\widehat{\Gamma}_{in}(f_0) = 0$. In the following discussion, we identify the factors that play a role in achieving this result

In his analysis of an aperture-coupled cavity, Collin [15] defines critical coupling as the matched condition at resonance when the cavity's input impedance equals the characteristic impedance of the waveguide. This is actually a very general definition of critical coupling, and the one we will use in the following analysis, although our cavity design utilizes loop coupling. Applying this definition to equation (1) means that we require

$$\widehat{Z}_{in}(f_0) = Z_0. \quad (7)$$

We also have that

$$\widehat{Z}_{in}(f_0) = \jmath X_s + R_0. \quad (8)$$

Since Z_0 is a real number based on the assumption of lossless transmission lines, these results imply that in order to satisfy the requirement in (7), two conditions must be met: $R_0 = Z_0$ and $X_s \to 0$.

Applying these conditions to the cavity when loaded by an external circuit, we have from (3)

$$\lim_{X_s \to 0} \kappa|_{R_0 = Z_0} = 1. \quad (9)$$

(Limits are used because the loop reactance X_s cannot physically be set equal to zero.) Equation (9) is the standard definition for critical coupling as derived from circuit models used to analyze resonant cavity modes. For the loaded frequency f_L in (6),

$$\lim_{X_s \to 0} f_L|_{R_0=Z_0} = f_0.$$

This result is significant because it says that, to the extent that we can minimize the effect of X_s, the resonant frequency measured at the input port will closely approximate f_0.

Finally, if the two limiting processes described above are applied to $\widehat{\Gamma}_{in}$ from (2), then we have the important result that

$$\lim_{X_s \to 0} \widehat{\Gamma}_{in}(f_0)\Big|_{R_0=Z_0} = 0$$

(since $\widehat{\Gamma}_d \to -1$ as $X_s \to 0$.)

V. Critical Coupling

The coupling factor κ is often used as a design specification when describing the required performance of a resonant cavity. However, this algebraic quantity, derived from simple circuit models, does not completely characterize the necessary design limits needed for optimum performance. If an application requires the resonant structure to be operated at critical coupling, then as we've seen in the previous section, it isn't enough to require that $\kappa = 1$. Specifically, it is possible to obtain a value of $\kappa = 1$ under less-than-optimal coupling conditions. This can be demonstrated by conducting numerical experiments using the equations derived from the one-port circuit model. In Figs. 4 and 5, calculations of $\widehat{\Gamma}_{in}$ from Eq. (2) for different values of X_s are shown. For each of these curves, the coupling factor $\kappa = 1$; however, as $X_s \to 0$, the null of the magnitude response of $\widehat{\Gamma}_{in}$ moves closer and closer to the unloaded resonance at $f_0 = 10$ GHz. On the Smith Chart plot in Fig. 5, the impedance at resonance approaches Z_0. As will be shown later, these effects are even more pronounced with measurement data.

These numerical calculations based on the simple circuit model reinforce the idea that the reactance of the coupling loop needs to be minimized as much as possible to achieve optimal performance. The problem is that the reactance is a physical property of the loop, and can't be directly changed once it is built. However, by using parallel matching networks, there is a way to reduce the loading of the loop's reactance. In the next section, we describe a two-step process that can be used to achieve this result with almost any resonant structure.

VI. Impedance Control Through Matching Networks

The results of the previous sections demonstrate that in order to achieve optimum performance of the cavity's response at resonance, two things must happen to Z_{in}: $R_0 \to Z_0$ and $X_s \to 0$. The practical steps needed to accomplish these goals are very similar to those required in the impedance matching problems encountered in antenna design [6], [16]. As shown in Fig. 6, an impedance matching network composed of a

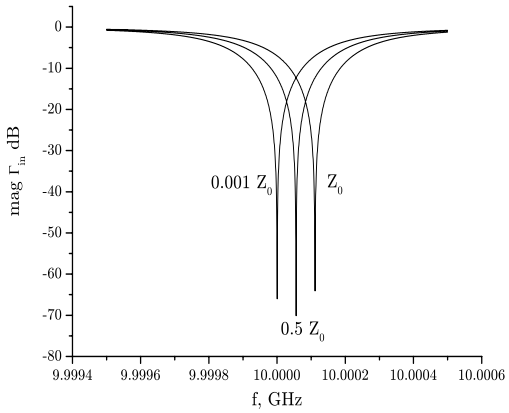

Fig. 4. Magnitude data calculated from $\widehat{\Gamma}_{in}$ with different values of X_s (i.e., $X_s = Z_0, X_s = 0.5Z_0, X_s = 0.001Z_0$). For all curves, $\kappa = 1$, $f_0 = 10$ GHz, and $Q_0 = 45000$.

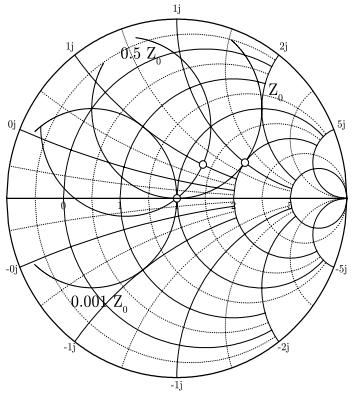

Fig. 5. Smith Chart data calculated from $\widehat{\Gamma}_{in}$ with different values of X_s (i.e., $X_s = Z_0, X_s = 0.5Z_0, X_s = 0.001Z_0$). For all curves, $\kappa = 1$, $f_0 = 10$ GHz, and $Q_0 = 45000$. The unloaded resonant frequency f_0 is indicated with $\circ$.

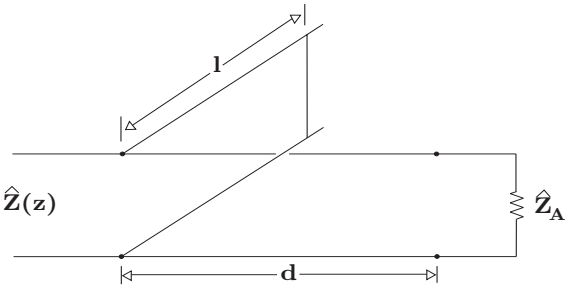

Fig. 6. Circuit schematic of the matching network for a transmission line with line impedance $\widehat{Z}(z)$ connected to an antenna with load impedance $\widehat{Z}_A$.

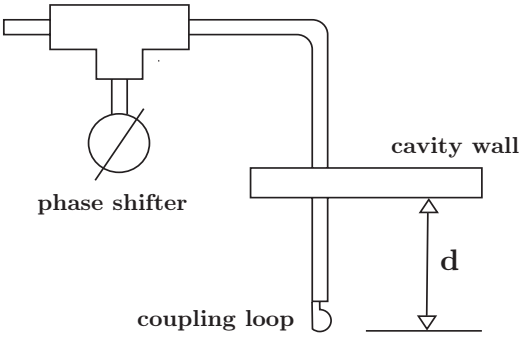

Fig. 7. Coupling loop matching in a resonant cavity analogous to the antenna matching configuration in Fig. 6 (loop depth *d* is exaggerated for clarity.)

shorted stub in parallel with an antenna load impedance $\widehat{Z}_A$ is used to match the antenna to the transmission line. By locating the matching stub at the correct distance *d*, the real part of the input impedance is matched to the characteristic impedance of the transmission line. Adjustment of the stub length *l* so that its parallel admittance cancels the admittance of the antenna load completes the process, presenting a matched impedance to the transmission line at the reference plane.

The algorithm we employ in our matching scheme for critically coupled cavities is analogous to the antenna matching problem. As shown in Fig. 7, the depth of the coupling loop into the cavity is adjusted so that, close to f_0, the real part of the input impedance at the measurement reference plane is approximately Z_0 and the imaginary part is very small. The coaxial T-junction (shown in Figs. 1 and 8) allows connection of a tuning device in parallel to the cavity so that it plays a role similar to the shorted stub in impedance matching for an antenna. Specifically, the tuning device's susceptance must be of the opposite sign as the loop susceptance in order to cancel out its effect. Our design uses an electronic phase shifter as the tuning device, which as an added benefit, allows for servo control of the cavity response in order to optimally maintain the minimum value of $\widehat{\Gamma}_{in}(f_0)$.

VII. Input and Output Matching Designs

There are two basic approaches to implementing the impedance matching methods previously discussed. The first design configures the matching network at the input port of the cavity, as shown in Fig. 1. Since the input port is set at critical coupling, this approach offers the advantage of greater control of input impedance through variations of the phase shifter. However, for input signals of relatively high power, electronic phase shifters cannot generally be used and so it is preferable to use an alternative design, as shown in Fig. 8. The phase shifter is located at the output port, which allows input signals of higher power to be used, but requires greater coupling values in order to effectively control the input impedance of the cavity. The phase shifter can be terminated with different loads for different effects, but in practice, we terminate with either a short or an open.

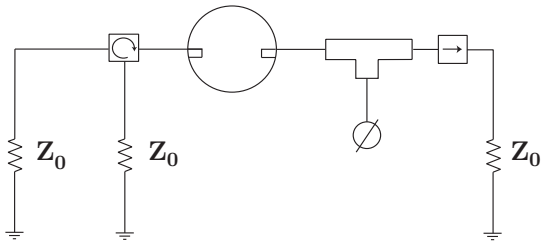

Fig. 8. Simplified diagram of cavity circuit with output matching. Z_0 is the system's characteristic impedance.

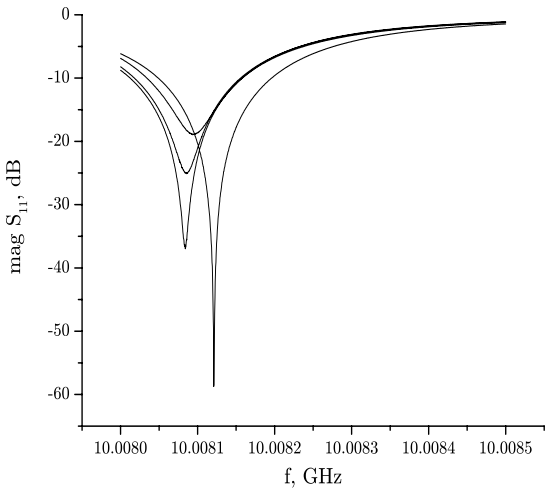

Fig. 9. Measured data of $|S_{11}|$ at 10 GHz for different values of the variable phase shifter shown in Fig. 8.

VIII. Measurement Data

Two cavities of different designs were measured in order to demonstrate the ideas presented in the previous sections. As stated initially, both cavities are constructed of aluminum and plated internally with silver. (Note: the resonant frequency of each cavity was engineered to be slightly high in order to allow for temperature tuning with a servo-controlled heater.) Using the output matching scheme shown in Fig. 8, a 10 GHz cavity operating in the TE_{023} mode produced the data shown in Figs. 9 - 11. The three curves in each figure were produced by varying the phase shifter connected to the output port until the measured impedance at the input reference plane was equal to Z_0 at f_0. This can be seen on the Smith Chart of Fig. 11 where the lower curve intersects the center point (normalized Z_0) at f_0. The magnitude plot in Fig. 9 reveals a deep null at this matched condition, approaching the asymptotic value of $\widehat{\Gamma}_{in} = 0$ (or $-\infty$ in dB). In Fig. 10, we see the dramatic improvement in the phase response of the cavity when the matched condition is achieved. This is also indicative of the discriminator curve obtainable with this matching technique.

A cavity operating at 40 GHz using the TE_{015} mode was measured using the input matching configuration shown in Fig.

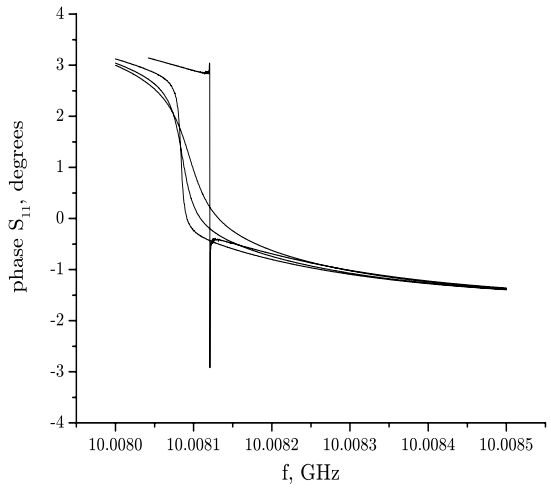

Fig. 10. Measured phase of S_{11} at 10 GHz for different values of the variable phase shifter shown in Fig. 8.

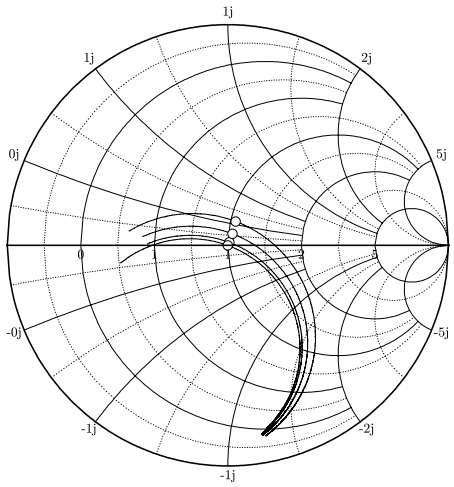

Fig. 11. Measured Q circle data of the input impedance of the 10 GHz cavity, plotted on the Smith Chart to demonstrate the tuning effect of the variable phase shifter. The resonant frequency f_L is indicated by $\circ$.

1. Data at 40 GHz for this cavity's response are plotted in Figs. 12 and 13, clearly demonstrating that these results are obtainable at higher frequencies.

IX. Conclusion

We have described an impedance matching technique for resonant cavities that allows the cavity's input impedance to be controlled with a variable phase shifter. This leads to an optimization of the cavity's response at the resonant frequency, in essence nulling out the effect of the coupling loop's reactance with respect to the input reference plane. We have used a simple circuit model of the cavity's resonant mode to explain how this procedure works, following closely a similar approach used in impedance matching methods with antennas. These results are general in nature, and could be applied to almost any other resonant structure (e.g., dielectric resonators on planar circuits, waveguide-coupled cavities, etc.) And finally, we presented measured datum using cavities operating at 10 GHz and 40 GHz that confirm the concepts developed with the circuit model and realized with the matching network.

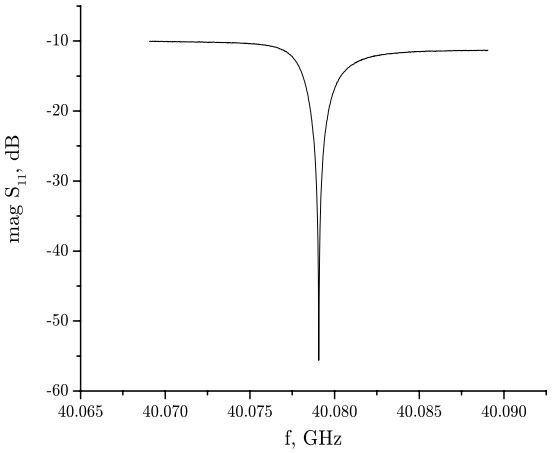

Fig. 12. Measured data of $|S_{11}|$ using a 40 GHz cavity.

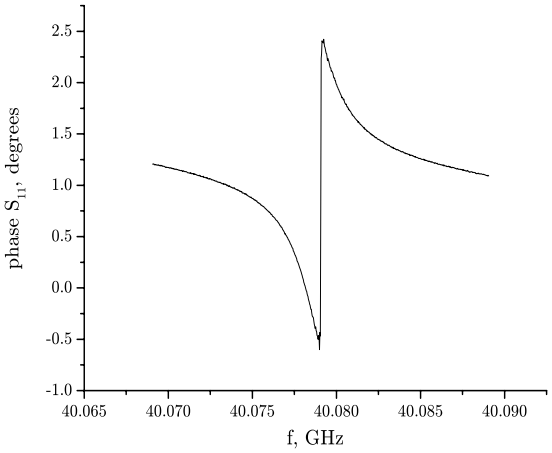

Fig. 13. Measured phase of S_{11} using a 40 GHz cavity.

References

[1] A. S. Gupta, D. A. Howe, C. W. Nelson, A. Hati, F. L. Walls, and J. F. Nava, "High spectral purity microwave oscillator: Design using conventional air-dielectric cavity," *IEEE Transactions on Ultrasonics, Ferroelectrics, and Frequency Control*, vol. 51, no. 10, pp. 1225–1231, October 2004.

[2] A. L. Whitwell and N. Williams, "A new microwave technique for determining noise spectra at frequencies close to the carrier," *Microwave J.*, pp. 27 – 32, November 1959.

[3] J. G. Ondria, "A microwave system for measurement of AM and PM noise spectra," *IEEE Trans. Microwave Theory Tech.*, vol. 16, no. 9, pp. 767 – 781, 1968.
[4] F. L. Walls, "Suppressed carrier based PM and AM noise measurement techniques," *Proc. IEEE Int. Freq. Contr. Symp.*, pp. 485–492, 1997.
[5] J. G. Hartnett, M. E. Tobar, and E. N. Ivanov, "Novel interferometric frequency discriminators for low noise microwave applications," *IEEE Trans. Ultrason., Ferroelect., Freq. Contr.*, vol. 48, no. 3, May 2001.
[6] C. T. A. Johnk, *Engineering Electromagnetic Fields and Waves*, 2nd ed. John Wiley & Sons, Inc., 1988.
[7] C. G. Montgomery, R. H. Dicke, and E. M. Purcell, Eds., *Principles of Microwave Circuits*. McGraw-Hill Book Company, 1947.
[8] E. L. Ginzton, *Microwave Measurements*. McGraw-Hill Book Company, 1957.
[9] M. E. Tobar and D. G. Blair, "A generlaized equivalent circuit applied to a tunable sapphire-loaded superconducting cavity," *IEEE Trans. Microwave Theory Tech.*, vol. 39, no. 9, September 1991.
[10] J. G. Hartnett, "Secondary frequency standards: Frequency-temperature compensated resonator design and improved frequency discriminators," Ph.D. dissertation, University of Western Australia, 2000, chapter 5.
[11] D. Kajfez, *Q Factor*. Vector Fields, 1994.
[12] R. L. Lewis, "Relative permittivity measurement of rectangular copper-laminated substrates using the full-sheet resonance technique," National Institute of Standards and Technology, NISTIR 5062, April 1997.
[13] K. Leong and J. Mazierska, "Precise measurements of the Q factor of dielectric resonators in the transmission mode - accounting for noise, crosstalk, delay of uncalibrated lines, coupling loss, and coupling reactance," *IEEE Trans. Microwave Theory Tech.*, vol. 50, no. 9, September 2002.
[14] H. A. Atwater, "Reflection coefficient transformations for phase-shift circuits," *IEEE Trans. Microwave Theory Tech.*, vol. 28, no. 6, pp. 563–568, June 1980.
[15] R. E. Collin, *Foundations for Microwave Engineering*, 2nd ed. McGraw-Hill, Inc., 1992.
[16] C. A. Balanis, *Antenna Theory*, 2nd ed. John Wiley & Sons, Inc., 1997.